ChemistrySelect

Research Article
doi.org/10.1002/slct.202201331

Chemistry Europe
European Chemical Societies Publishing

www.chemistryselect.org

Decorating Porous Aromatic Framework Cavities with Long-Chain Alkyl Grippers for Rapid and Selective Iron(III) Detection

Zhuojun Yan,[a] Jialin Xie,[a] Tongfei Geng,[a] Bin Feng,[a] Bo Cui,[a] Na Li,[a] Pinjie Su,[b] Naishun Bu,*[b] Ye Yuan,*[c] and Lixin Xia*[a, d]

Due to the key role of Fe(III) species in living organisms, real-time detection of Fe^{3+} ions is an important topic for the accurate diagnosis of many diseases, such as Alzheimer's, Huntington's, and Parkinson's diseases. Here, soft long-chain alkyl groups serving as the grippers are introduced into the rigid porous skeleton through a one-step Suzuki-coupling reaction. Through the ion-induced dipole interaction of long-chain alkyl groups with Fe^{3+} ions, the resulting PAF solid exhibits excellent enrichment effect for metal elements. Accordingly, an absorption competition quenching (ACQ) phenomenon is observed leading to the selectivity and sensitivity for monitoring Fe^{3+} ions in the presence of various interfering ions. The sensing performance with the detection limit of 5.34×10^{-6} M far exceeds that of other porous solids including MOFs, ZIFs, COPs, and PNTs, etc. This work pioneers an efficient strategy that introducing long-chain alkanes as the grippers for the design of advanced sensors for practical application.

Introduction

Iron is a vital metallic element in biological system, widely involved in oxygen metabolism, DNA/RNA replication, and hemoglobin formation in the living organisms. The excessive variation of Fe^{3+} ions concentration in the body leads to many diseases, such as iron deficiency anemia (IDA), Alzheimer's disease, Huntington's disease, and Parkinson's disease.[1–5] World Health Organization (WHO) suggests that the proper concentration of Fe^{3+} species in drinking water should be below 3×10^{-4} mg mL^{-1}.[6] Since the concentration monitoring became increasingly important, many detection methods are developed including atomic absorption spectroscopy, liquid chromatography, inductively coupled plasma mass spectrometry, and time-of-flight resonance ionization mass spectrometry.[7] The fluorescence sensing with certain advantages of high selectivity, simple operation, short response time, and low cost is considered as a promising approach for practical application.[8,9] As a vital component, fluorescent materials are fundamentally interested and practically demanded for selective detecting Fe^{3+} ions at low concentrations.

Porous aromatic frameworks (PAFs) are built through a bottom-up strategy using rigid organic monomers with a predesigned geometry via irreversible C–C bonds into amorphous networks.[10] These solids are known for the ultra-large surface area, tailorable structure, and high thermal/chemical/oxidation stability, which are conducive to many valuable applications such as catalysis, ion/molecule storage, and gas separation.[11–13] Recently, molecular imprinting technology (MIT) is integrated into the construction of PAF architecture, producing binding sites with a specific geometry and size for the selective complement of a template object.[14–17] The open framework provides large accessible surface for the decoration of specified sites and intrinsic pathways for rapid mass transfer.[18–20] All these results demonstrate the huge potential of PAF materials for the realization of highly selective and sensitive detection of Fe^{3+} ions.

Pyrene and its derivatives are important polycyclic aromatic hydrocarbons that are widely used as a fluorescent sensor.[21,22] However, the conjugated building units tend to tightly pack in porous solids, leading to the decrease of fluorescence quantum yield and limited application scopes. Herein, long-chain alkanes were innovatively introduced into the PAF networks, which greatly improved the fluorescence quantum yield from 0.79% (pure phenyl-based PAF) to 22.98% (long-chain alkane-grafted PAF). Based on the absorption competition quenching effect, the resulting sample achieves high sensitivity and selectivity for fluorescent detection of Fe^{3+} ions. This work provides some inspirations for the synthesis of PAF fluorescence sensor with

[a] *Dr. Z. Yan, J. Xie, T. Geng, B. Feng, B. Cui, N. Li, Prof. L. Xia*
College of Chemistry
Liaoning University
110036 Shenyang, Liaoning (P. R. China)
E-mail: lixinxia@lnu.edu.cn
[b] *P. Su, Dr. N. Bu*
School of Environmental Science
Liaoning University
110036 Shenyang, Liaoning (P. R. China)
E-mail: bunaishun@lnu.edu.cn
[c] *Prof. Y. Yuan*
Key Laboratory of Polyoxometalate and Reticular Material Chemistry of Ministry of Education, Faculty of Chemistry
Northeast Normal University
130024 Changchun, Jilin (P. R. China)
E-mail: Yuany101@nenu.edu.cn
[d] *Prof. L. Xia*
Liaoning Key Laboratory of Chemical Additive Synthesis and Separation
Yingkou Institute of Technology
115014 Yingkou, Liaoning (P. R. China)

Supporting information for this article is available on the WWW under https://doi.org/10.1002/slct.202201331

Scheme 1. (a) Synthetic routes for LNU-22 and LNU-24; (b) Schematic diagram of LNU-24 fluorescent sensing Fe^{3+} ions.

high fluorescence quantum yield, which will attract wide attention from materials science and sensing fields.

Results and Discussion

Description of structure

Through a Suzuki-coupling reaction, 9,9-dioctylfluorene-2,7-diboronic acid bis(pinacol) ester was utilized as the building monomer for the introduction of long-chain alkyl chains (C-8) in the rigid porous skeleton, denoted LNU-24. For comparison sake, pure phenyl-based porous architecture was synthesized using 1,3-phenyldiboronic acid bis(pinacol) ester as a reference, named as LNU-22 (Scheme 1).

Both FT-IR and solid-state ^{13}C-NMR spectra were performed to verify the structural integrity of the prepared LNU-22 and LNU-24. Compared with the raw monomers, the disappearance of B–O (at 1368 cm^{-1}) and C–Br (at 495 cm^{-1}) bands implied the completeness of the Suzuki-coupling reaction (Figure 1a and 1b).[23] Similarly, there was an elongated peak observed that was assigned to the C–H vibration (at 2930 cm^{-1}) of the long-chain alkane on the PAF skeleton.[24] As detected by the solid-state ^{13}C-NMR spectroscopy (Figure S1a and S1b), the characteristic peaks within the region of $\delta = 115 \sim 155$ ppm belonged to the aromatic carbon atoms on the substituted or unsubstituted benzene rings. On the basis of that, the chemical shifts of $\delta = 20 \sim 40$ ppm were ascribed to the alkyl chains of LNU-24 solid. All these shreds of evidence in both FT-IR and solid-state ^{13}C-NMR spectra demonstrate the successful synthesis of PAF networks.

Figure 1. FT-IR spectra for (a) LNU-22 and (b) LNU-24; (c) N_2 adsorption-desorption isotherms and (d) NL-DFT pore size distribution curves for LNU-22 and LNU-24.

The thermal stability of fluorescent materials is crucial for the service life of fluorescent sensors.[25] As shown in Figure S2, the thermogravimetric analysis illustrates the excellent thermal stability of PAF samples up to 350 °C. Compared with LNU-22, the apparent weight loss of LNU-24 in the range of 350 ~ 500 °C is due to the escape of long alkyl chains from the porous polymer.[24,26] In addition, LNU-22 and LNU-24 are insoluble or undecomposed in methanol, ethanol, tetrahydrofuran, dichloromethane, chloroform, and other common solvents,

proving that these samples possess excellent chemical stability for practical detecting applications.[27,28] Due to the irreversible coupling process of the metal-catalyzed Suzuki coupling reaction, the powder X-ray diffraction patterns indicate that LNU-22 and LNU-24 have non-ordered structures (Figure S3).[23,24,29–32] The peaks observed in the PXRD patterns for both LNU-22 and LNU-24 are ascribed to the Si substrates. SEM images depict that LNU-22 and LNU-24 are composed of irregularly stacked nanospheres with a dominant particle diameter in the range of 0.2 ~ 1 μm (Figure S4a and S4b). TEM images show the worm-like textures of LNU-22 and LNU-24 (Figure S4c and S4d).

As shown in Figure 1c, a large hysteresis loop between adsorption and desorption isotherms for LNU-22 ($0.05 < P/P_0 < 1$), indicating the hierarchical porous structure.[33–35] Similar results can be observed from the pore size distribution diagram (Figure 1d) that the pore size of LNU-22 locates in the range of 0.78 ~ 1.44 nm (micropores) and 2.15 ~ 3.85 nm (mesopores). Compared with the adsorption curve of LNU-22, LNU-24 shows a small hysteresis loop and a relatively low adsorption rise curve in the low pressure region (Figure 1c), indicating the existence of mesoporosity.[33,34] Correspondingly, the pore size distribution of LNU-24 is mainly distributed in 3.78 ~ 5.68 nm. These wide pore size distributions for LNU-22 and LNU-24 are attributed to that (1) the vacuum environment causes the collapsed pore architecture during the test; (2) the irreversible coupling reaction produce a large amount of structural defects leading to the formation of meso- and macro- pores. The specific surface area was calculated based on Brunauer-Emmett-Teller (BET) model. The surface areas of LNU-22 and LNU-24 were determined to be 524 and 71 $m^2 g^{-1}$, respectively. The obviously reduced BET surface area of LNU-24 is attributed to that the long-chain alkanes occupied the pore cavities inside the PAF architecture.[24]

Study of optical properties

Fluorescence emission spectra of LNU-22 and LNU-24 solids were measured under the excitation wavelength of 365 nm. The maximum emission wavelengths of LNU-22 and LNU-24 located at 480 and 508 nm, respectively, corresponding to blue-green and yellow-green colors (Figure 2a). In addition, the absolute quantum yield of fluorescence (Φ_{FL}) of PAF powder was analyzed by steady-state transient fluorescence spectra, and the Φ_{FL} values of LNU-22 and LNU-24 were 0.79% and 22.98%, respectively. The difference in both luminescence colors and quantum yield of the two PAF polymers was attributed to the grafted alkyl chains inhibited the layered packing of conjugated fluorene units in the LNU-24 sample.[36]

Selective detection of Fe^{3+} ions against other interfering ions including Ag^+, Co^{2+}, Ni^{2+}, Al^{3+} et al. is necessary for practical application in the human body.[37] 2 mg PAF powder (LNU-22 or LNU-24) was dispersed in 5 mL THF solvent after that 1 mL nitrate solution with a concentration of 0.01 mol L^{-1} was poured into the mixture. The quenching effect of LNU-22 or LNU-24 on different metal ions was monitored by the luminescence intensity in the emission spectrum of the

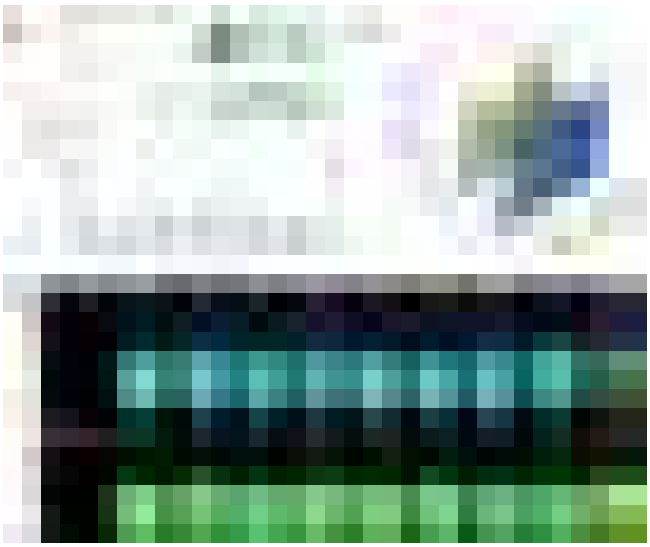

Figure 2. (a) Fluorescence spectra of LNU-22 and LNU-24 solids at an excitation wavelength of 365 nm (insert: luminescence photographs of LNU-22 and LNU-24 powders before and after irradiation by $\lambda_{ex} = 365$ nm portable UV lamp); (b) The emission intensities of LNU-22 and LNU-24 suspensions in THF solution after addition of 0.01 mol L^{-1} $M(NO_3)_x$ ($M^{x+} = Ag^+$, Ni^{2+}, Hg^{2+}, Pb^{2+}, Cu^{2+}, Co^{2+}, Al^{3+}, Fe^{3+}); (c) The PL quenching photographs by adding metal ions into LNU-22 and LNU-24 suspensions in THF solution, where PL is excited under $\lambda_{ex} = 365$ nm using portable UV lamp.

suspension. As shown in Figure 2b, the luminescence intensity of both LNU-22 and LNU-24 was significantly quenched after added Fe^{3+} ions. A visual color change of the PAF sample was monitored in THF under UV-light before and after the addition of nitrate solution, and only Fe^{3+} ions obviously quenched the fluorescence performance of the two PAFs (Figure 2c). These phenomena indicated that LNU-22 and LNU-24 could be used as fluorescent sensor to detect Fe(III) elements. LNU-24 with double long-chain alkane groups revealed a higher quantum yield and a better quenching effect than LNU-22, which was selected as the preferred object.

In order to better understand the sensing mechanism of LNUs for Fe^{3+} ions, fluorescence titration experiments were carried out by enlarging the concentration of Fe^{3+} ions. As Fe^{3+} ions concentration increases, the fluorescence intensity gradually decreases (Figure 3a and 3b). As to other interfering ions, the competitive experiments were conducted under the same conditions but with different metal ions (Ag^+, Ni^{2+}, Hg^{2+}, Pb^{2+}, Cu^{2+}, Co^{2+}, and Al^{3+}). As observed in Figure 3c and 3d, there was no apparent intensity change in the presence of interfering ions only. On the contrary, 1 mL of Fe^{3+} ions solution with a concentration of 0.01 mol L^{-1} was added to a suspension containing interfering ions, the fluorescence of PAF sample was immediately quenched, suggesting the high selectivity of PAF powder for Fe^{3+} ions. These experiments prove that LNUs possess huge potential for the selective detection of Fe^{3+} ions.

The selective quenching mechanism of LNUs was carefully studied. It was found that the quenching capability of LNUs for Fe^{3+} ions was attributed to the absorption competitive quenching mechanism.[6,38,39] As shown in Figure 4a, there was

Figure 3. Emission spectra of (a) LNU-22 and (b) LNU-24 suspensions in THF solution with increased amounts of Fe^{3+}; The fluorescence intensity of (c) LNU-22 and (d) LNU-24 in THF after the addition of Fe^{3+} and other metal ions.

Figure 4. (a) UV-Vis absorption spectrum of Fe^{3+} ions and fluorescent emission spectra of LNU-22 and LNU-24; (b) UV-Vis absorption spectra of LNU-22, LNU-24 and Fe^{3+} ions.

no overlap between the UV-Vis absorption spectrum of Fe^{3+} ions and the emission spectra of LNUs, proving that no energy transfer between Fe^{3+} ions and LNUs. Based on the light-emitting mechanism, the electrons inside the luminescent material will transition from a stable ground state to an unstable excited state and then return to the ground state, during which energy is released in the form of fluorescence.[39] As shown in Figure S9, other ions except Fe^{3+} did not observe obvious absorption peaks in the range of 250 ~ 500 nm, indicating that other metal ions have poor light absorption ability in this wavelength range. As shown in Figure 4b, the UV-Vis absorption spectra of Fe^{3+} (analyte) and LNUs (luminophore) in the range of 250 ~ 500 nm have obvious overlap, which leads to the absorption competition between the PAF sample and Fe^{3+} ions for the light source energy, resulting in the fluorescence quenching.[6]

As shown in Figure S10, the quenching coefficients for the two PAF materials are calculated according to the Stern-Volmer formula: $I_0/I = K_{SV}[C] + 1$ (I_0 is the initial fluorescence intensity, I standing for the fluorescence intensity after quenching; K_{SV} is quenching coefficient, and $[C]$ is the molar concentration of analyte).[40–43] In order to better understand the fluorescence quenching mechanism of materials, we fitted the relative fluorescence intensity of LNU-22 and LNU-24 with Fe^{3+} concentration. As shown in Figure S10, the Stern Volmer curves of LNU-22 and LNU-24 show a good linear relationship at low concentrations, indicating that the fluorescence quenching mechanism of the PAF materials is static quenching.[44,45] The PAF sensor combines with Fe^{3+} ions to form a stable non-fluorescent complex, which leads to the fluorescence quenching result.[46] The K_{SV} values of two PAF polymers are calculated to be 8.80×10^2 and 2.13×10^3 M^{-1}, respectively. The bigger K_{SV} value of LNU-24 indicates that the higher sensitivity for Fe^{3+} ions compared with LNU-22.[4] It is mainly because of the long-chain alkanes serving as the grippers, forming a complex with metal ions *via* ion/induced dipole interactions.[47] Based on this interaction, the alkyl chains capture Fe^{3+} ions from the solution and then transfer them into the PAFs cavities. The increased local concentration of metal ions enhances the competition efficiency of PAFs and Fe^{3+} ions, which consequently evidences the ultrahigh sensitivity. FT-IR further confirmed the interaction between iron ion and long chain alkanes. As shown in Figure S11, the characteristic peaks for alkyl groups at 2960 cm^{-1} moved to 2953 cm^{-1}, indicating the obvious interaction between Fe^{3+} and the long alkyl chain in LNU-24.

Further, the limit of detection (LOD) was analyzed by using the equation as follows: $LOD = 3\sigma/k$ and $k = \Delta I/\Delta C$,[43,48] where σ is the standard deviation of fluorescence intensity without the analyte. ΔI is the different values between fluorescence intensity with and without the analyte added; ΔC is difference value of the analyte concentration. The LOD values of LNU-22 and LNU-24 were calculated to be 2.86×10^{-5} M and 5.34×10^{-6} M, which was much lower than some previously reported luminescent materials such as MOFs, COPs, ZIFs and PNTs, etc. (Table 1) [4,6,7,39,43,49–59], indicating the outstanding capability of PAF sample for sensing Fe^{3+} ions.

Stability is important for fluorescent sensing materials from an economic and ecological point of view. LNU-24 can be recovered from Fe^{3+} ions in THF/H_2O dispersion by simple ethanol washing and drying. It is worth noting that the quenching efficiency of LNU-24 on Fe^{3+} ions reaches up to 92.11% of the original value after five consecutive sensing-cycles (Figure S12), indicating that LNU-24 has good cycling stability as a fluorescence sensor.

Conclusion

In summary, soft long-chain alkyl groups were introduced in the rigid porous skeleton as the grippers through the one-step Suzuki-coupling reaction. The grafted long-chain alkyl groups will form a complex with metal ions via ion/induced dipole interactions. Due to the enrichment effect, the resulting PAF architecture reveals excellent selectivity and outstanding luminescence quenching for Fe^{3+} ions in the presence of various interfering ions. This article shows the great potential of flexible group-decorated porous sensor for ion monitoring and expands the application scopes of fluorescent PAF materials.

Table 1. Comparison of other materials for Fe^{3+} sensing.

Material	K_{sv} (M^{-1})	Dection limit (M)	Ref.
LNU-22	8.80×10^{2}	2.86×10^{-5}	This work
LNU-24	2.13×10^{3}	5.34×10^{-6}	This work
$[Cd_2Na(L)(BDC)_{2.5}]\cdot9H_2O$	1.67×10^{4}	–	[4]
$[Cd_2(L)(2,6\text{-}NDC)_2]\cdot DMF\cdot5H_2O$	1.44×10^{4}	–	[4]
$[Cd_2(L)(BPDC)_2]\ DMF\cdot9H_2O$	1.08×10^{4}	–	[4]
PNT-2	2.0186×10^{4}	3.1×10^{-5}	[6]
PNT-3	2.3982×10^{4}	5.07×10^{-5}	[6]
PAF-5CF	1.1865×10^{4}	3.8×10^{-5}	[7]
COP-6	1.1004×10^{4}	–	[39]
COP-7	6.375×10^{3}	–	[39]
COP-9	1.6875×10^{4}	–	[39]
SXNU-J1	4.0693×10^{3}	3.391×10^{-6}	[43]
SXNU-J2	5.2628×10^{3}	3.677×10^{-6}	[43]
EuL_3	4.1×10^{3}	5×10^{-4}	[49]
BUT-14	2.17×10^{3}	3.8×10^{-6}	[50]
$\{[Cd(L)(BPDC)]\cdot2H_2O\}_n$	3.63×10^{4}	2.21×10^{-6}	[51]
$\{[Cd(L)(SDBA)(H_2O)]\cdot0.5H_2O\}_n$	3.59×10^{4}	7.14×10^{-6}	[51]
$\{[Zn(ATA)(L)]\cdot H_2O\}_n$	0.557×10^{3}	3.76×10^{-6}	[52]
$[Tb(HL)(DMF)(H_2O)_2]\cdot3H_2O$	4.479×10^{3}	5×10^{-5}	[53]
N-CDs	2.0958×10^{3}	0.96×10^{-6}	[54]
NID FONPs	3.5×10^{3}	1.25×10^{-5}	[55]
4-poly[9,9′-(N-carbazole-hexyl) fluorene]	1.4×10^{7}	5×10^{-6}	[56]
poly[2,7-(9-(2-ethyloctyl)-carbazole)]	1.8×10^{4}	–	[56]
TT-COF	5.63×10^{3}	8.4×10^{-5}	[57]
PMDA-TAPB	1.087×10^{4}	3.61×10^{-5}	[58]
1α-DMF	1.92×10^{4}	1.80×10^{-7}	[59]

Experimental Section

Material

1,3,6,8-Tetrabromopyrene, 1,3-phenyldiboronic acid bis(pinacol) ester and 9,9-dioctylfluorene-2,7-diboronic acid bis(pinacol) ester were purchased from Energy Chemical. Tetrakis(triphenylphosphine)palladium(0) $[Pd(PPh_3)_4]$ was obtained from TCI. All materials were used without further purification.

Synthesis of LNUs

1,3,6,8-Tetrabromopyrene (301 mg, 0.579 mmol) and 1,3-phenyldiboronic acid bis(pinacol) ester (382 mg, 1.158 mmol) were added to a two-neck flask equipped with a condenser. Then N,N′-dimethylformamide (60 mL) was injected through a syringe, and liquid nitrogen was used to cool the mixture to below 0 °C, then the system was purged with N_2 by three nitrogen-pump cycles. Potassium carbonate solution (2 M, 5 mL) and tetrakis(triphenylphosphine)palladium (40 mg, 0.035 mmol) were quickly added into the bottle, experiencing three nitrogen-pump cycles, the mixture was stirred at 130 °C for 48 h under N_2. After cooled to room temperature, the solid was obtained by suction filtration. Washing sequentially with water (2×35 mL), N,N′-dimethylformamide (2×35 mL), tetrahydrofuran (2×35 mL), acetone (2×35 mL) to remove unreacted monomers and catalyst residues, further purification was carried out by Soxhlet extraction with tetrahydrofuran (24 h), trichloromethane (24 h), and dichloromethane (24 h). Finally, the product was dried in a vacuum environment for 24 h at 90 °C to give the LNU-22 powder (90% yield). The synthetic process for LNU-24 (81% yield) is the same as the LNU-22, using 9,9-dioctylfluorene-2,7-diboronic acid bis(pinacol) ester (744 mg, 1.158 mmol) to replace 1,3-phenyldiboronic acid bis(pinacol) ester.

Characterization

Fourier transform infrared spectroscopy (FT-IR) was conducted using a Shimadzu-Prestige21 spectrometer in the wavenumber region of 400 ~ 4000 cm^{-1}. ^{13}C solid-state CP/MAS NMR was measured on a Bruker AVANCE III model 400 MHz NMR spectrometer at a MAS rate of 5 kHz. Powder X-ray diffraction (PXRD) data was recorded on a Bruker D8 ADVANCE diffractometer with Cu–Kα radiation, $2\theta = 5°$ up to 60°. Scanning electron microscopy (SEM) was examined on a SU8010 model scanning electron microscope with an accelerating voltage of 5 kV. Transmission electron microscopy (TEM) was obtained on a JEM-2100 with an accelerating voltage of 200 kV. Thermogravimetric analysis (TGA) was investigated by METTLER TOLEDO TGA/DSC 2 thermal analyzer under nitrogen atmosphere at the heating rate of 10 °C min^{-1}. N_2 adsorption/desorption isotherms were measured by a Micromeritics ASAP 2460 instrument. Ultraviolet-Visible (UV-Vis) absorption spectra were recorded on a Perkin-Elmer Lambda 35. All fluorescence data were recorded on a VARIAN CARY Eclipse FL750.

Supporting Information Summary

The supporting information for this article contains characterization data, calculations and supplementary figures mentioned in the results and discussion section.

Acknowledgements

This work was supported by National Key Research and Development Project of China (2018YFC1801200); National Natural Science Foundation of China (31972522, 21704037, 21671089); Liaoning Revitalization Talents Program (XLYC2007032, XLYC2002097); Major Science and Technology Project of Liaoning Province (2019JH1/10300001); Scientific Research Fund of Liaoning Provincial Education Department (LQN202003, L2020002); Liaoning Provincial Natural Science Foundation (2021-MS-149, 2020-YKLH-22).

Conflict of Interest

The authors declare no conflict of interest.

Keywords: fluorescent quenching · iron ion · long-chain alkyl · porous aromatic framework · sensor

[1] M. F. Zhang, J. Han, H. P. Wu, Q. Wei, G. Xie, S. P. Chen, S. L. Gao, *RSC Adv.* **2016**, *6*, 94622–94628.
[2] S. Pal, P. K. Bharadwaj, *Cryst. Growth Des.* **2016**, *16*, 5852–5858.
[3] Y. Q. Zhang, X. D. Li, L. J. Gao, J. H. Qiu, L. P. Heng, B. Z. Tang, L. Jiang, *ChemPhysChem* **2014**, *15*, 507–513.
[4] D. Zhao, X. H. Liu, Y. Zhao, P. Wang, Y. Liu, M. Azam, S. I. Al-Resayes, Y. Lu, W. Y. Sun, *J. Mater. Chem. A* **2017**, *5*, 15797–15807.
[5] L. H. Cao, F. Shi, W. M. Zhang, S. Q. Zang, T. C. W. Mak, *Chem. Eur. J.* **2015**, *21*, 15705–15712.

[6] M. Wang, L. Guo, D. P. Cao, *Sci. China Chem.* **2017**, *60*, 1090–1097.
[7] T. T. Ma, X. Zhao, Y. Matsuo, J. Song, R. Zhao, M. Faheem, M. Chen, Y. F. Zhang, Y. Y. Tian, G. S. Zhu, *J. Mater. Chem. C* **2019**, *7*, 2327–2332.
[8] S. Y. Zhu, B. Yan, *Dalton Trans.* **2018**, *47*, 1674–1681.
[9] H. B. Wan, Q. F. Xu, P. Y. Gu, H. Li, D. Y. Chen, N. J. Li, J. H. He, J. M. Lu, *J. Hazard. Mater.* **2021**, *403*, 123656.
[10] Y. Yuan, Y. J. Yang, G. S. Zhu, *EnergyChem* **2020**, *2*, 100037.
[11] Y. Yuan, G. S. Zhu, *ACS Cent. Sci.* **2019**, *5*, 409–418.
[12] Y. Yuan, Y. J. Yang, G. S. Zhu, *ACS Cent. Sci.* **2020**, *6*, 1082–1094.
[13] Z. J. Yan, H. Ren, H. P. Ma, R. R. Yuan, Y. Yuan, X. Q. Zou, F. X. Sun, G. S. Zhu, *Microporous Mesoporous Mater.* **2013**, *173*, 92–98.
[14] Y. J. Yang, D. Deng, S. L. Zhang, Q. H. Meng, Z. N. Li, Z. Y. Wang, H. Y. Sha, R. Faller, Z. Bian, X. Q. Zou, G. S. Zhu, Y. Yuan, *Adv. Mater.* **2020**, *32*, 1908243.
[15] Z. J. Yan, Y. Yuan, Y. Y. Tian, D. M. Zhang, G. S. Zhu, *Angew. Chem. Int. Ed.* **2015**, *54*, 12733–12737; *Angew. Chem.* **2015**, *127*, 12924–12928.
[16] Y. Yuan, Y. J. Yang, M. Faheem, X. Q. Zou, X. J. Ma, Z. Y. Wang, Q. H. Meng, L. L. Wang, S. Zhao, G. S. Zhu, *Adv. Mater.* **2018**, *30*, 1800069.
[17] Y. J. Yang, Z. J. Yan, L. L. Wang, Q. H. Meng, Y. Yuan, G. S. Zhu, *J. Mater. Chem. A* **2018**, *6*, 5202–5207.
[18] Y. Yuan, Q. H. Meng, M. Faheem, Y. J. Yang, Z. N. Li, Z. Y. Wang, D. Deng, F. X. Sun, H. M. He, Y. H. Huang, H. Y. Sha, G. S. Zhu, *ACS Cent. Sci.* **2019**, *5*, 1432–1439.
[19] Z. Y. Wang, Q. H. Meng, R. C. Ma, Z. K. Wang, Y. J. Yang, H. Y. Sha, X. J. Ma, X. H. Ruan, X. Q. Zou, Y. Yuan, G. S. Zhu, *Chem* **2020**, *6*, 1683–1691.
[20] Y. Yuan, F. X. Sun, F. Zhang, H. Ren, M. Y. Guo, K. Cai, X. F. Jing, X. Gao, G. S. Zhu, *Adv. Mater.* **2013**, *25*, 6619–6624.
[21] K. Ayyavoo, P. Velusamy, *New J. Chem.* **2021**, *45*, 10997–11017.
[22] L. X. Xia, H. C. Zhang, B. Feng, D. Q. Yang, N. S. Bu, Y. B. Zhao, Z. J. Yan, Z. N. Li, Y. Yuan, X. J. Zhao, *Chem. J. Chinese U.* **2019**, *40*, 2456–2464.
[23] Y. B. Zhao, N. S. Bu, H. M. Shao, Q. Zhang, B. Feng, Y. M. Xu, G. Y. Zheng, Y. Yuan, Z. J. Yan, L. X. Xia, *New J. Chem.* **2019**, *43*, 18158–18164.
[24] Y. B. Zhao, Y. Yuan, Y. M. Xu, G. Y. Zheng, Q. Zhang, Y. Q. Jiang, Z. Y. Wang, N. S. Bu, L. X. Xia, Z. J. Yan, *Nanoscale* **2021**, *13*, 1961–1969.
[25] H. T. Wu, H. Xu, F. R. Tao, X. Su, W. W. Yu, T. D. Li, Y. Z. Cui, *New J. Chem.* **2018**, *42*, 12802–12810.
[26] Y. L. Chen, F. H. Li, Z. S. Bo, *Macromolecules* **2010**, *43*, 1349–1355.
[27] L. Zhang, J. S. Sun, F. X. Sun, P. Chen, J. Liu, G. S. Zhu, *Chem. Eur. J.* **2019**, *25*, 3903–3908.
[28] J. Y. Weng, Y. L. Xu, W. C. Song, Y. H. Zhang, *J. Polym. Sci. Part A* **2016**, *54*, 1724–1730.
[29] T. M. Geng, D. K. Li, Z. M. Zhu, Y. B. Guan, Y. Wang, *Microporous Mesoporous Mater.* **2016**, *231*, 92–99.
[30] S. J. Xu, J. He, S. B. Jin, B. E. Tan, *J. Colloid Interface Sci.* **2018**, *509*, 457–462.
[31] S. J. Yang, X. S. Ding, B. H. Han, *Macromolecules* **2018**, *51*, 947–953.
[32] Y. F. Xu, C. Zhang, P. Mu, N. Mao, X. Wang, Q. He, F. Wang, J. X. Jiang, *Sci. China Chem.* **2017**, *60*, 1075–1083.
[33] Y. C. Li, W. Z. Li, Z. H. Cheng, Y. He, H. M. Li, H. X. Li, Y. Z. Liao, *ChemNanoMat* **2020**, *6*, 58–63.
[34] W. J. Du, Y. C. Qin, C. L. Ni, W. L. Dai, J. P. Zou, *ACS Appl. Polym. Mater.* **2020**, *2*, 5121–5128.
[35] T. M. Geng, W. Y. Zhang, Z. M. Zhu, G. F. Chen, L. Z. Ma, S. N. Ye, Q. Y. Niu, *Polym. Chem.* **2018**, *9*, 777–784.
[36] L. L. Han, H. X. Jiang, D. Ouyang, W. C. Chen, T. Hu, J. Y. Wang, S. G. Wen, M. L. Sun, R. Q. Yang, *Nano Energy* **2017**, *36*, 110–117.
[37] X. J. Ma, Y. J. Yang, R. C. Ma, Y. F. Zhang, X. Q. Zou, S. J. Zhu, X. Ge, Y. Yuan, W. Zhang, G. S. Zhu , *Chem. Sci.* **2020**, *11*, 12187–12193.
[38] L. L. Wang, C. X. Yang, X. P. Yan, *Sci. China Chem.* **2018**, *61*, 1470–1474.
[39] L. Guo, X. F. Zeng, J. H. Lan, J. Yun, D. P. Cao, *ChemistrySelect* **2017**, *2*, 1041–1047.
[40] T. M. Geng, Z. M. Zhu, X. Wang, H. Y. Xia, Y. Wang, D. K. Li, *Sens. Actuators B* **2017**, *244*, 334–343.
[41] S. S. Nagarkar, A. V. Desai, S. K. Ghosh, *Chem. Commun.* **2014**, *50*, 8915–8918.
[42] Z. J. Yan, J. N. Liu, C. K. Miao, P. J. Su, G. Y. Zheng, B. Cui, T. F. Geng, J. T. Fan, Z. Y. Yu, N. S. Bu, Y. Yuan, L. X. Xia, *Molecules* **2022**, *27*, 126.
[43] W. J. Ji, W. W. Pei, Q. B. Wang, G. F. Liu, B. Yan, S. Q. Yao, Q. G. Zhai, *J. Solid State Chem.* **2019**, *274*, 18–25.
[44] V. Prakash, R. Bhar, S. Sharma, S. K. Mehta, *RSC Adv.* **2019**, *9*, 22320–22326.
[45] D. D. Zhang, X. T. Tian, H. H. Li, Y. P. Zhao, L. Chen, *Colloids Surf. A* **2021**, *608*, 125563.
[46] E. Ciotta, P. Prosposito, R. Pizzoferrato, *J. Lumin.* **2019**, *206*, 518–522.
[47] R. Chen, L. Li, *J. Am. Soc. Mass Spectrom.* **2001**, *12*, 367–365.
[48] S. Nandi, H. Reinsch, S. Banesh, N. Stock, V. Trivedi, S. Biswas, *Dalton Trans.* **2017**, *46*, 12856–12864.
[49] M. Zheng, H. Q. Tan, Z. G. Xie, L. G. Zhang, X. B. Jing, Z. C. Sun, *ACS Appl. Mater. Interfaces* **2013**, *5*, 1078–1083.
[50] B. Wang, Q. Yang, C. Guo, Y. X. Sun, L. H. Xie, J. R. Li, *ACS Appl. Mater. Interfaces* **2017**, *9*, 10286–10295.
[51] S. G. Chen, Z. Z. Shi, L. Qin, H. L. Jia, H. G. Zheng, *Cryst. Growth Des.* **2017**, *17*, 67–72.
[52] B. Parmar, Y. Rachuri, K. K. Bisht, E. Suresh, *Inorg. Chem.* **2017**, *56*, 10939–10949.
[53] S. T. Zhang, J. Yang, H. Wu, Y. Y. Liu, J. F. Ma, *Chem. Eur. J.* **2015**, *21*, 15806–15819.
[54] T. N. J. I. Edison, R. Atchudan, J. J. Shim, S. Kalimuthu, B. C. Ahn, Y. R. Lee, *J. Photochem. Photobiol. B* **2016**, *158*, 235–242.
[55] D. Sarkar, M. Chowdhury, P. K. Das, *J. Mater. Chem. B* **2021**, *9*, 494–507.
[56] P. Li, Y. Zhao, L. Yao, H. R. Nie, M. Zhang, *Sens. Actuators B* **2014**, *191*, 332–336.
[57] T. Zhang, A. Salah, S. H. Chang, Z. Zhang, G. Wang, *Tetrahedron* **2021**, *96*, 132405.
[58] X. Liang, Z. J. Ni, L. M. Zhao, B. Ge, H. Zhao, W. Z. Li, *Microchem. J.* **2021**, *170*, 106663.
[59] Y. W. Huang, P. M. Chuang, J. Y. Wu, *Inorg. Chem.* **2020**, *59*, 9095–9107.

Submitted: April 8, 2022
Accepted: September 15, 2022